$Ba_xSr_{1-x}TiO_3$ NANOCRYSTALLINE THIN FILMS DEPOSITION GROUNDED IN RF MAGNETRON CO-SPUTTERING

J. RESÉNDIZ-MUÑOZ[a], J. L. FERNÁNDEZ-MUÑOZ[b,*], J. R. FARIAS-MANCILLA[c], M. MELENDEZ-LIRA[d], J. J. MEDEL-JUÁREZ[e], O. ZELAYA-ANGEL[d]

[a]*Chemical-Engineering, COARA—Autonomous University of San Luis Potosí, Matehuala City, San Luis Potosi, Mexico.*

[b]*National Polytechnic Institute, CICATA-IPN Legaria, Calzada Legaria Str., No. 694, Col. Irrigación, Z.P. 11500, Mexico City, Mexico.*

[c]*Institute of Engineering and Technology, Department of Physics and Mathematics, Autonomous University of Ciudad Juárez, Chihuahua, Mexico*

[d]*Department of Physics. Center for Research and Advanced Studies of the National Polytechnic Institute (CINVESTAV), Av. IPN 2508. Zacatenco, Z.P. 07000, Mexico City, México.*

[e]*Computer Research Center of the National Polytechnic Institute (CIC-IPN), Av. Juan de Dios Bátiz, Esq. Miguel Othón de Mendizábal, Col. Nueva Industrial Vallejo, Prov. Gustavo A. Madero, Z.P. 07738, Mexico City, Mexico.*

A solid solution of barium-strontium titanate $Ba_xSr_{1-x}TiO_3$ was deposited in thin films by RF reactive co-sputtering for x values within $0 \leq x \leq 1$. The films composition was controlled through applied RF power to $BaTiO_3$ and $SrTiO_3$ targets. The Ba and Sr contents in thin films is characterized through x values as a function of applied RF power showing a good concordance, within the experimental error, with a kinetic description based on a molecular free path mean sputtering process. The elemental composition of the films was obtained considering the electron dispersion spectroscopy, and the x value inferred through the change of the (110) lattice inter-planar spacing. This one was obtained from the peak position in the x-ray diffraction (XRD) patterns by BSTO films. The average crystal size for the whole composition is around 20 nm, obtained from XRD data analysis.

(Received April 30, 2018; Accepted August 17, 2018)

Keywords: Sputtering deposition, thin films, stoichiometric behavior, Barium Strontium Titanate, Boltzmann's equation

1. Introduction

Materials property designs such as band gap, hardness, melting point, etc., in one form can be realized through alloying. The nano-metric perovskite oxides alloys have created a great interest due to the possibility to achieve better performance in applications such as solar cells, photo-catalysis, resistive memories and sensors [1-3]. The crystalline structure similarity between $BaTiO_3$ (BTO) and $SrTiO_3$ (STO) motivated by $Ba_xSr_{1-x}TiO_3$ (BSTO) deposit alloy modulating properties such as ferroelectricity and band gap between BTO and STO [4, 5]. Additionally, BSTO properties control is obtained through the deposition of thin films, due to the presence of stress or nano-structure formation [6]. BSTO films can be deposited by diverse techniques, such as sol-gel, RF sputtering, laser ablation and molecular beam epitaxy techniques [7-10].

In this work, the proportional characterization results between Ba and Sr content to determine x values in the BSTO films, along the entire $0 \leq x \leq 1$ range, deposited by reactive RF co-sputtering are presented. The Ba and Sr content versus the applied RF power follows a

*Corresponding author: jlfernandez@ipn.mx

sigmoidal function. The final films composition was controlled by the applied RF power to BTO and STO targets. Sifted diffraction peaks confirmed the successful production of BSTO solid solutions. Even so, the reactive co-sputtering process involves many parameters is shown illustratively in figure results the deposition behavior, in an acceptable sense, employing a kinetic energy gaseous model. The BSTO films methodology reported so far using applied RF power allows to apply the composition control.

2. Experimental details

BSTO films were deposited on 1.5 x 2.5 cm^2 quartz substrates by RF reactive means co-sputtering employing a cylindrical stainless-steel chamber with a diameter and a height of 36 cm and 24 cm, respectively. Substrates were supported on a circular stainless-steel holder (radius of 8 cm) rotating at 100 rpm and located at 8 cm from the two sputtering guns. An off-axis configuration was employed with 3 cm separation between the sputtering gun axes. The chamber was evacuated to pressure better than $1.2x10^{-3}$ Pa. afterwards; flushing was applied using 3.9 Pa of Argon (Ar) during 10 minutes. The reactive working atmosphere was a mixture of Ar/O_2 with a ratio $Ar/O_2 = 9$ at a 3.9 Pa. Both, Argon (Ar) and Oxygen (O_2) gases were ultra-high purity grade. The source materials were 2" targets of 99.95% BTO and 99.9% STO (SCI Engineered Materials, Inc). Prior to the films deposition targets were subjected during 15 minutes of a pre-sputtering process. 100% STO films (x=0) were obtained applying 120 W to the STO target and no applied RF power to the BTO target. 100% BTO films (x=1) were obtained using the inverse procedure. Values in the $0 \leq x \leq 1$ interval for the BSTO films were obtained changing the applied RF power to each target in 15 W steps in a complementary form, always keeping the total applied RF power to both targets at 120W. The films were deposited employing a 549 °C temperature of the substrate. The chemical composition was analyzed with a Scanning Electron Microscope (SEM) Jeol JSM-5300 equipped with a Kevex Energy Dispersive Spectrometer (EDS) model Delta 1calibrated using a standard semiconductor. The electron energy to 15 KeV, enough to excite the Lα X-ray emission with respect the interested materials, proving the film considered. The samples thickness were normalized to one min of growth and employing the SCOUT [11] program, obtaining the transmission spectra (not shown here). The X-ray diffractograms were obtained by a Phillips X´Pert diffractometer using the CuK $\alpha=1.54060$ Å wavelength. In order to calculate the particle size, the Full Width at Half Maximum (FWHM) of the (110) X-ray diffraction peak for each composition obtained a deconvolution procedure employing Gaussian profiles; the peak center obtained also. The particle size was measured using the Scherrer's formula: $d=0.9\,\lambda/(b\cos\theta)$; where λ is the wavelength of the X-Ray radiation, b is the FWHM of the peak, and θ the Bragg´s angle. For data analysis, the Origin 8 software was utilized.

3. Results and discussion

Figure 1 presents the BSTO deposit set samples, in which all films show the perovskite cubic structure. The peaks positions from x=0 (STO) to x=1 (BTO) for $Ba_xSr_{1-x}TiO_3$, change the composition of the film, without appreciate increments through the FWHM. The XRD pattern characteristics aforementioned indicate that the gradual incorporation of Ba in the STO lattice, and vice versa, preserves the perovskite structure without promoting structural disorder, indicating successful substitutional incorporation. In a sensitive XRD volume, it is plausible to assume that the films are mainly formed by BSTO alloy as there is no evidence of the superposition of BTO or STO diffractograms on those of the BSTO alloy. Figure 1 inset shows the behavior of the XRD peak associated to (110) plane as the composition of the samples changes from BTO to STO ($\Delta[2\theta] \cong 31.5°$ to 32.5°) [12, 13]. Figure 2 shows a linear connection between the (110) inter-planar distances of BTO and STO (green line) considering that the lattice parameter of the BSTO alloy follows the Vegard´s law [13, 14]. In the same figure, the values of the applied RF power to the BTO target as a function of (110) inter-planar spacing are shown. Figure 2 is employed

obtaining the values of the composition (x), extrapolating the Vegard's law and linear relation. Once, the x values are determined the molar concentration be calculated. Figure 3 presents the normalized concentrations $xM_{BTO}/(M_{BTO}+M_{STO})$ and $(1\text{-}x)M_{STO}/(M_{BTO}+M_{STO})$ with molecular masses: M_{BTO} = 233.192 g/mol and M_{STO} = 183.490 g/mol, displayed as a power function. Both concentration averages are also included. Observe in the lower inset that the average curve does not reproduce the real distribution of x vs P because it shows a symmetrical distribution of x values around x = 0.5. The top inset exhibits the non-normalized molar concentrations of both materials versus P, the difference of molecular masses in the concentration x values is observed. A sigmoid curve in cell dimensions versus Ba molar concentration in $Ba_xSr_{1-x}TiO_3$ has been previously reported by Chen and co-workers [15].

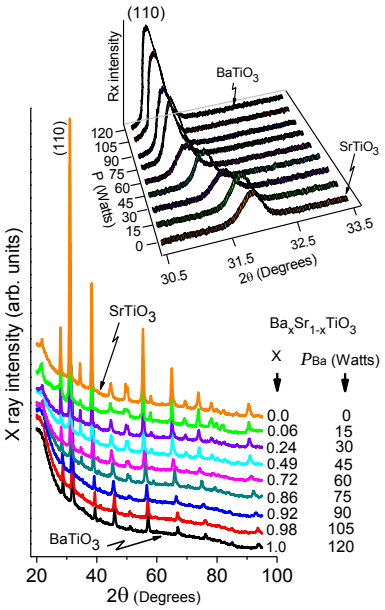

Fig. 1. X-Ray BSTO thin films diffract-grams deposited using RF reactive co-sputtering. Numbers on the right correspond to the x and P values. The inset shows the peak shift for the 110 plane as the composition changes.

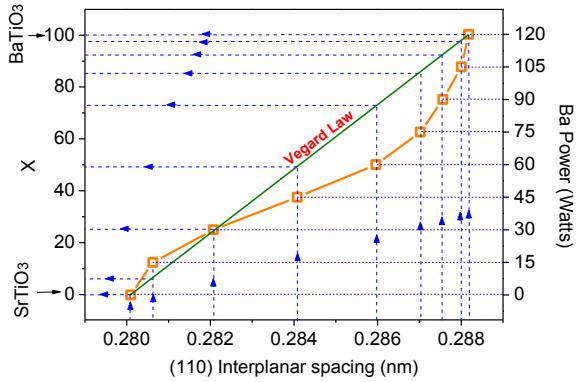

Fig. 2. The straight green line corresponds to the Vegard's law for the BSTO solid solution. The square symbols correspond to the interplanar spacing values for the 110 peak obtained from the XRD patterns. The curve is adjusted to aid to the eye. Broken lines identify the BSTO films assigned composition considering the Vegard's law. The vertical right axis corresponds to the BTO target power.

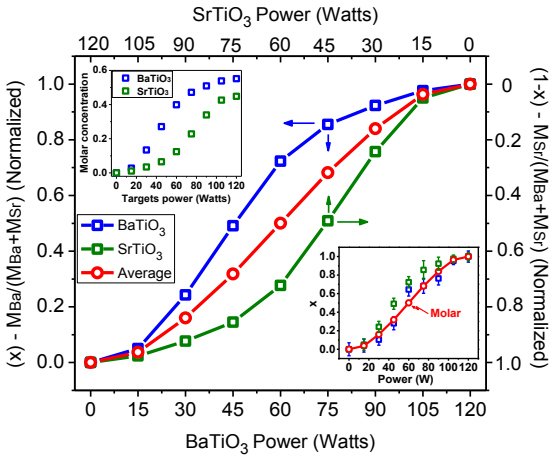

Fig. 3. Normalized molar concentration, left axis [$M_{Ba}x/(M_{Ba} + M_{Sr})$], right axis [$M_{Sr}(1\text{-}x)/(M_{Ba} + M_{Sr})$], vs. $BaTiO_3$ applied RF power. M_{Ba} = 233.19 g/mol and M_{Sr} = 183.19 g/mol are $BaTiO_3$ and $SrTiO_3$ molecular masses, respectively in which the top inset shows both the non-normalized molar concentrations vs. the power applied. The lower inset exhibits the average molar curve vs P along with experimental data.

Thin film production using a sputtering process involves many parameters that physical description seems unreachable, especially for compounds materials. However, there is a very active theoretical work trying to identify the relevant parameters that could describe this process achieving a tight control of thin film properties. A model describing the interaction between ions and plasma in Direct Current (DC) and high power pulsed magnetron sputtering for monoatomic materials has been proposed by J. Geiser and S. Blankenburg [16]. It can be considered that refereeing to the ionization process; RF sputtering is similar to DC because the sputtered material is ionized in a small proportion. The ions are mainly those found in the plasma, i.e., Argon (Ar) and Oxygen (O_2), are modulated into a deposition process.

On the other hand, BTO and STO compounds have similar crystallographic and chemical bond characteristics suggesting, as a first approximation. That the BSTO films study properties may be described for BTO (x) or STO (1-x) content in the films, showing that the RF reactive sputtering deposition process, of the quaternary BSTO films, is closely described by a modified Geiser and Blankenburg model calculating the BTO and STO proportional content in the films. It is assumed that BTO and STO molecules are the most components removed from the target by the Argon (Ar) ions impinging the targets.

The model proposed by Geiser and Blankenburg describes the sputtering deposition process in terms of the mean free path ions and is employed here considering (1) [16]:

$$\lambda = \frac{3}{4\pi} \frac{s}{\{\left(s+\frac{1}{2s}\right)\mathrm{erf}(s)+\frac{1}{\sqrt{\pi}}\exp(-s^2)\}} \frac{k_B T}{(R_{mol}+R_{gas})^2 P_{gas}} \quad (1)$$

Where λ means molecule free path that moves through like an ideal gas law, with kinetic energy $E = 1/2M_{mol}v^2$, where ν is the velocity of the relative molecules (projectile) with respect to ideal gas velocity background atoms (atoms of plasma), moving by sputtering-gas. R = radius, T = temperature, P = pressure, k_B = Boltzmann constant. To avoid confusion, it is necessary to emphasize that the model describes the particles ejected movement from the sputtered target-material going through the plasma. Then the sub-indexes "mol" refer to molecules ejected from the target, and "gas" to plasma (mostly Ar ions), respectively. The non-dimensional s parameter is defined in (2) as

$$s = [(M_{gas}/M_{mol})E/k_B T]^{1/2} \quad (2)$$

Where, $E = 1/2M_{mol}v^2$. This expression indicates that λ is a function of $E^{1/2}$, i.e., to molecule velocity, which is valid considering the projectile as a free particle among interactions [16, 17]. In this work, it is assumed that the kinetic energy of the sputtered molecules is directly proportional to the power, $E \propto P$. This assumption is supported by the fact that the sputtering deposition rate increases when the applied RF power also increases [18-20]. In this sense, for a component, $s = A'[(M_{gas}/M_{mol})P/k_BT]^{1/2}$, where A' is a constant. Extra consideration to be taken into account is: the probability of N particles, moving through a gaseous medium with a mean free path λ, that are able to travel a distance δ without suffering a collision, described in Eq. (3) as:

$$N'(\delta) = N_o' exp(-\delta/\lambda) \tag{3}$$

Where, N_o' is the particles number given a distance δ and the time interval [21]. The proposal in this work, is to know if the number of molecules required by substrate from the target, is proportional to the molecule mean free path, and to the probability that a given number of them $N(d)$ obtained the substrate, that is: $N(d) = N_o\lambda exp(-d/\lambda)$. Where N_o is the number of molecules emerging, in a time interval, from the target and d a distance representing the target-substrate distance. The object of this work is to know that the relationship can also be interpreted x as a given type of molecule in the film expressing as $x = A''\lambda exp(-d/\lambda)$, A'' being constant. Since λ is a function of P, where the change in composition is a well-defined power function. In this form, the molecules rate (particles per unity power) change its content, depending on the applied RF power on target, calculated as follows: $dx = (dx/dP)dP = A''[d\{\lambda\exp(-d/\lambda)\}/dP]dP$. Due to data P in discrete form, with integration region (ΔP) with P constant around each datum, the value is assumed. Therefore, $\Delta x = \int dx = A''\int[d\{\lambda\exp(-d/\lambda)\}/dP]dP$, and the integration should be carried out in the ΔP intervals as shown by bars-plot in the lower inset of Figure 4, where P values are the data used by BSTO films deposition. The first derivate $d[\lambda\exp(-d/\lambda)]/dP$ is also constant along each interval, then $x = \Delta x = A''[d\{\lambda\exp(-d/\lambda)\}/dP]\,\Delta P$, being A'' an adjustable constant. This result indicates that in the case where ΔP is constant, x is directly proportional to the first derivative of $\lambda\exp(-d/\lambda)$ with respect to P, obtaining $x = A\mathrm{dj}[\lambda\exp(-d/\lambda)]/dP$, and A as a constant to normalize to the unit. The top inset displays λ, provided by the model, of BTO and STO molecules versus P (right axis), and the $\lambda_{STO}/\lambda_{BTO}$ ratio (left axis) whose values are around 1.34. The fact is a consequence of the molecular masses ratio M_{BTO}/M_{STO} =1.27. The sigmoidal path is followed by the calculous obtained from this approximation, after normalized, illustrated in Figure 4 where P is used to obtain BTO films. The line was drawn only as a guide. The differentiation was achieved using the Origin 8 software. The sigmoidal concentration profile versus applied RF power reflects, after all, the storage of the particles number, disappearing from the target-substrate path, and very fast particles produce collision cascades which also disperse them away.

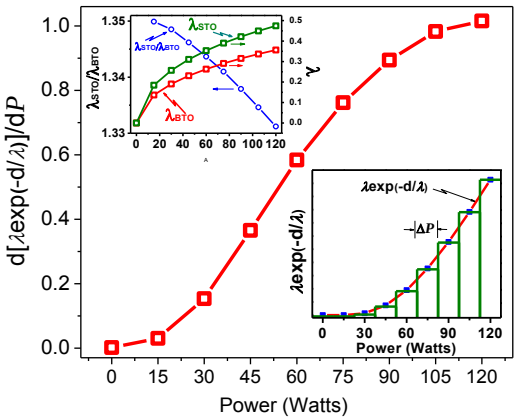

Fig. 4. Experimental values of P substituted in the $d[\lambda exp(-d/\lambda)]/dP$. Lines are adjusted by eliminating the visual effects. The top inset shows the λ values for BTO and STO molecules (right axis), and the $\lambda_{STO}/\lambda_{BTO}$ ratio (left axis). The lower inset illustrates the $\lambda exp(-d/\lambda)$ vs P function (blue points and red lines). Bars delimited the integration identify zones.

The experimental data for BTO (x) and STO (1-x) content obtained from XRD and EDS measurements are plotted as a function of P in Figure 5. The result obtained from the model is represented in orange and green open squares, respectively. Both curves are very close which suggests that an average curve can represent the result. The top inset displays the average points of both data set are calculated from the model obtaining films with a specific composition using the applied RF power as a control parameter. The lower inset exhibits the average curves for the model, and that for molar concentration; both sigmoid curves are very close. However, the data distribution is contained in the model prediction. The concordance indicates that for this system the sputtering process is mainly dominated by the interaction among the Ar, $BaTiO_3$ and $SrTiO_3$ ions (considering molecular dipolar momentums). The fact that the experimental composition values of Ba and Sr obtained from two different techniques fit in a reasonable manner, could indicate in the sputtering process is mainly described like a kinetic process. XRD data measurements determine the x values coupling the EDS measurements model prediction.

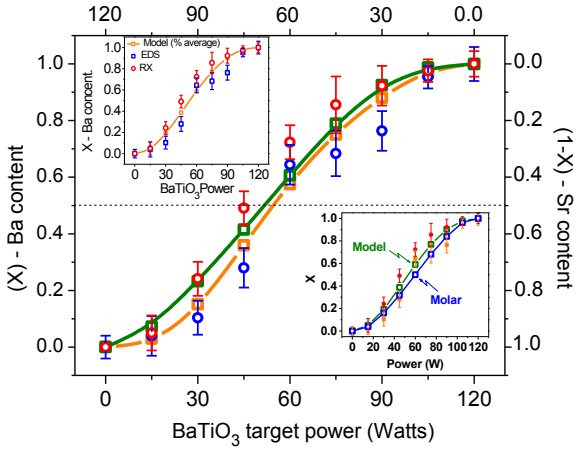

Fig. 5. Circles correspond to compositional values obtained from the the XRD patterns (red) analysis and the EDS techniques (blue) for the BSTO thin films. The point-line curves correspond to the fitting obtained employing the theoretical model $x \alpha d[\lambda exp(-d/\lambda)]/dP$, using the assumptions. Lines are an aid to eye. The top inset illustrates the average results of BTO and STO (red point-line) model. The lower inset displays the x values comparison considering the molar calculation.

The films were deposited maintaining all the growing parameters constants except the applied RF power. The main difficulty was describing the relation between E and P in Equation (2). For this reason, a direct proportion $E = \kappa P$ was proposed, and different κ values were assayed obtaining a functional approximation. The fitting determination is proportional between to BTO and STO content as a function of the applied RF power carried out replacing P instead of E in Equation 2, and the molecular masses of $BaTiO_3$ and $SrTiO_3$ (233.19 and 189.49 g/mol, respectively). Actually, to get acceptable and reliable results for the λ values $M_{mol}/10$ and $E/100$ ($P/100$) should be used in Equation (2). Moreover, other combinations can also be tried, since the final data obtained from the model will be adjusted to experimental results. The molecular radii of $BaTiO_3$ and $SrTiO_3$ to be used in Equation (1), were considered approximately equals, then they were not taken into account for calculation. For the $exp(-d/\lambda)$ term, with the same above-aforementioned purpose, $d = 1.5$ for Ba concentrations was found after some attempts. In Figure 6, we can be observed that the experimental thickness values show how, under the same growing conditions, the 100%-$BaTiO_3$ film thickness is three times that for the 100%-$SrTiO_3$ (5.34 and 1.76 nm, respectively). This behaviour is reflected in the inset of Figure 1. As a matter of fact, the growth rate is not the same in both cases, and the rate not only depends on the BTO and STO mass difference, other properties significantly influence the compound material deposition. Again, to obtain adequate fitting parameters to reproduce the experimental line-shape of data points, the value of d in Equation (3) for Sr was fitted to 2.432, obtained after a recurrent iterative process.

The squared of the molecular masses ratio $(M_{BTO}/M_{STO})^2 = (233.192/183.490)^2 = 1.615 \cong 1.621 = 2.432/1.5$, where 1.5 and 1.432 are the values used for d in $x = Ad[\lambda\exp(-d/\lambda)]/dP$ for BTO and STO, respectively, fitting. This result could mean that the probability to reach the substrate depends, in some way, on the molecular mass.

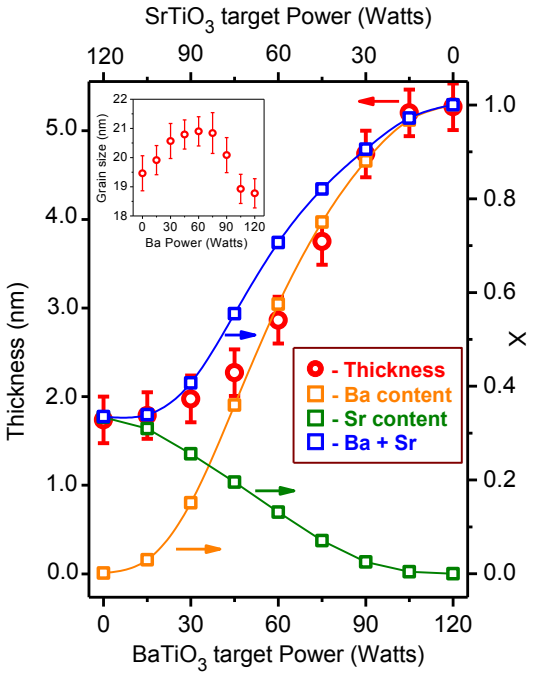

Fig. 6. Open squares represent Ba (orange) and Sr (green) content normalized to the Ba content (which was also normalize to the unit), against P. Blue open squares represent the Ba + Sr contents, that is the orange plus green data. Red points represent the experimental thickness of the BSTO films. The inset displays, the plot of the crystal size value obtained using Scherrer's analysis using XRD peak is associated with the 110 plane.

It is worth to remark that the experiment was designed in such a manner that the applied RF power to the BSTO target is complementary to that applied to the other target to maintain a total applied RF power value of 120 W. Then Ba concentration in the films increases as Sr concentration decreases. A similar behavior for the change in Sr concentration is expected, but with a rate of change in Sr content three times lower. This behavior occurs because the STO compound has a lower sputtering rate than that of BTO [22]. The larger growth rate of BTO than STO is reflected in Figure 2, where a greater number of BSTO films with Ba content $x > 0.5$ than the equivalent fact for Sr ($1\text{-}x > 0.5$) it is evident (5 and 3, respectively). Figure 6 also shows two Ba and Sr sigmoidal functions of both concentrations (orange and green curves, respectively), normalized to Ba content, against the applied RF power. The sum of these two sigmoidal functions is also plotted (blue curve), whose data-path it is expected to fit with that of the thickness data. The lack of an acceptable fitting, even within de error bars, can be probably due to some additional mutual dispersion of both types of molecules when co-sputtering is carried out. The inset of Figure 5 also shows the average crystal size obtained from the analysis of the FWHM of the (110) XRD peak versus applied RF power and the size values are distributed in the 18.5 -21 nm interval. The curve shows a maximum value close to the center of the power range (60 Watts). This zone is that where the deposition rate for both components as a function of P is maximum.

4. Conclusions

RF reactive co-sputtering process employing STO and BTO targets allowed the successful production of nanometric thin films of the solid solution BSTO in the whole range of x compositions. It was found that composition is easily controlled through the applied RF power to each target.

A close dependence description of all as a function of applied RF power to each target, according to J. Geiser and S. Blankenburg. The modified the model assuming a linear relationship between ions kinetic energy and applied RF power. The model obtains total control of the composition and film thickness of the BSTO films, adjusting the applied RF power. The satisfactory result obtained indicates that the sputtering process is related with the interaction with the inert gas ion and BTO and STO molecules.

Acknowledgements

We acknowledge to technical support of M. Guerrero, A. Guillen Cervantes and L. Lopez from Departamento de Fisica at Cinvestav-IPN. This work was partially supported by CONACyT and SECITI-CDMX. MML., and sabbatical CONACyT support.

References

[1] A. Bussmann-Holder, J. Phys: Condens. Matter **24**, 273202 (2012).
[2] C. Dubourdieu, J. Bruley, T. M. Arruda, A. Posadas, J. Jordan-Sweet, M. M. Frank, E. Cartier, D. J. Frank, S. V. Kalinin, A. A. Demkov, V. Narayanan, Nat. Nanotechnol. **8**, 748 (2013).
[3] J. C. Agar, S. Pandya, R. Xu, A. K. Yadav, Z. Liu, T. Angsten, S. Saremi, M. Asta, R. Ramesh, MRS Commun. **6**, 151 (2016).
[4] Y. Liu, S. Wang, Z. Chen, L. Xiao, Sci. China Mater. **5**, 851 (2016).
[5] U. Gleissner, C. Megnin, M. Benkler, D. Hertkorn, H. C. Elsenhmeier, K. Schumann, F. Paul, T. Hanemann, Ceram-Silikáty **60**, 1 (2016).
[6] V. K. Thakur, R. K. Gupta, Chem. Rev. **116**, 4260 (2016).
[7] S. U. Adikary, A. L. Ding, H. L. W. Chan, J. Phys. A. **75**, 597 (2002).
[8] T. Horikawa, N. Mikami, T. Makita, J. Tanimura, M. Kataoka, K. Sato, M. Nunoshita, Jpn. J. Appl. Phys. **32**, 4126 (1993).
[9] T. Nakamura, Y. Yamanaka, A. Morimoto, T. Shimizu, Jpn. J. Appl. Phys. **34**, 5150 (1995).
[10] A. J. Hauser, E. Mikheev, A. P. Kajdos, A. Janotti, Appl. Phys. Lett. **108**, 102901 (2016).
[11] SCOUT. W. Theiss: (Hard and Software, Aachen, Germany), www.mtheuss.com.
[12] R. K. Roeder, E. B. Slamovich, J. Amer. Ceram. Soc. **82**, 1665 (1999).
[13] Y. J. Kim, S. B. Rawal, S. D. Sung, W. I. Lee, Bull. Korean Chem. Soc. ***32***, 141 (2011).
[14] M. C. Gust, L. A. Momoda, N. D. Evans, M. L. McCartney, J. Am. Ceram. Soc. **84**, 1087 (2001).
[15] W. K. Chen, C. M. Cheng, J. Y. Huang, W. F. Hsieh, T. Y. Tseng, J. Phys. Chem. Solids **61**, 969 (2000).
[16] J. Geiser, S. Blankenburg, Commun. Comput. Phys. **11**, 1618 (2012).
[17] T. Nakano, S. Baba, Vacuum **51**. 485 (1998).
[18] S. Khorram, S. Sobhanian, H. Naghshara, J. Appl. Phys. **109**, 073305 (2011).
[19] A. R. Nyaiesh, L. Holland, Vacuum **31**, 315 (1981).
[20] S. Desa, S. Ghosal, R. L. Kosut, J. L. Ebert, T. E. Abrahamson, A. Kozak, D. W. Zou, X. Zhou, J. F. Groves, H. N. G. Wadley, J. Vac. Sci. Technol. A **17**, 1926 (1999).
[21] D. Mihalas, B. Weibel Mihalas, Dover Pub. Inc., N. Y. 2016, Chap. 3, p. 99.
[22] J. Olejnicek, Z. Hubicka, P. Virostko, A. Deyneka, L. Jastrabik, D. Chvostova, H. Sichova, J. Pokorny, Integ. Ferroel. **81**, 227 (2006).